On the Role of Hazard and Particle Failure Statistics on the Variation of Fracture Parameters of Ductile-Brittle Composites

Mikhail Lebyodkin, Tatiana Lebedkina

▶ **To cite this version:**

Mikhail Lebyodkin, Tatiana Lebedkina. On the Role of Hazard and Particle Failure Statistics on the Variation of Fracture Parameters of Ductile-Brittle Composites. Metals, 2019, 9 (6), pp.633. 10.3390/met9060633 . hal-02357180

HAL Id: hal-02357180
https://hal.science/hal-02357180

Submitted on 9 Nov 2019

HAL is a multi-disciplinary open access archive for the deposit and dissemination of scientific research documents, whether they are published or not. The documents may come from teaching and research institutions in France or abroad, or from public or private research centers.

L'archive ouverte pluridisciplinaire **HAL**, est destinée au dépôt et à la diffusion de documents scientifiques de niveau recherche, publiés ou non, émanant des établissements d'enseignement et de recherche français ou étrangers, des laboratoires publics ou privés.

Distributed under a Creative Commons Attribution 4.0 International License

metals

MDPI

Article

On the Role of Hazard and Particle Failure Statistics on the Variation of Fracture Parameters of Ductile-Brittle Composites

Mikhail Lebyodkin [1,*] and Tatiana Lebedkina [2]

[1] Laboratoire d'Etude des Microstructures et de Mécanique des Matériaux (LEM3), CNRS, Université de Lorraine, Arts & Métiers ParisTech, 7 rue Félix Savart, F-57000 Metz, France

[2] Center of Excellence "LabEx DAMAS", Université de Lorraine, 7 rue Félix Savart, F-57000 Metz, France; tleb1959@gmail.com

* Correspondence: mikhail.lebedkin@univ-lorraine.fr; Tel.: +33-0-3-72-74-77-71

Received: 13 May 2019; Accepted: 29 May 2019; Published: 31 May 2019

Abstract: The behavior of a simple computer model considering a random distribution of brittle spherical particles in a ductile matrix is examined in order to highlight the intrinsic variations of the fracture conditions due to the probabilistic nature of the particle cleavage. The model is qualitatively supported by experimental data on stress-strain behavior and damage accumulation in an Al-Si alloy with unconnected equiaxed Si particles. It is used to evaluate the effect of the particle failure statistics on the fracture characteristics (strength, ductility, and fraction of cracked particles) and their scatter, which occur to be strongly dependent on the specific shape of the probabilistic law. In particular, it is found that the variations of the fracture conditions may depend non-monotonously on its sharpness, in the case of the well-known Weibull statistics controlled by the value of the respective modulus of the material of hard particles. The existence of a maximum scatter leads to a suggestion that the choice of the reinforcements may influence not only on the average value of the fracture resistance but also on the quality of its prediction.

Keywords: metal matrix composites; fracture; aluminum alloys; statistical model

1. Introduction

Damage accumulation and the fracture of crystals involve various physical processes and remain one of the major problems of mechanical behavior of materials. Even for a pure polycrystalline material, one can distinguish ductile and brittle fracture, voids growth, transgranular and intergranular failure, shear band decohesion, crack nucleation due to twin interaction [1–5]. Non-homogeneous materials, such as metal-matrix composites, envisage yet a larger spectrum of failure modes, including cleavage of brittle particles embedded in a ductile matrix and matrix-particle decohesion [6–22].

The complexity and diversity of the pertinent physical processes, amplified by their dependence on the specific microstructure, have led to the development of various approaches to theoretical modeling. The fracture of brittle-ductile composites involves three main stages: void nucleation through particles cleavage and/or particle-matrix debonding, void growth necessitating the understanding of a coupling between plasticity and damage, and the final void coalescence leading to the ultimate fracture. Therefore, its modeling inevitably requires the so-called "local approach" [2], based on the physical mechanisms of the local damage and plastic flow as opposed to the global approach which describes the fracture via macroscopic failure criteria such as fracture toughness (e.g., [23]). Starting from the early theory of ductile rupture by void nucleation and growth [24], numerous efforts were made for the elaboration of continuum theories both in an analytical and numerical framework, using

micromechanics and phenomenological constitutive models [8,14–19,25–29]. This approach has largely contributed to the description of the above processes, understanding the role of the stress triaxiality, and prediction of the ductility and strength (see review [30]). In this framework, the numerical simulations were mainly based on the "void cell computations" suggesting either periodic arrays of cells with spherical particles or more complex (but also regular) arrangements including several families of cells of different size, cells containing several voids, and variation of the voids shape [26–31]. On the other hand, numerous experiments showed that the fracture of composites depend on the heterogeneous distribution of particle sizes, shapes, and interparticle spacing, as well as the associated topology of the second phase [6–13,16–22,32–34]. Models considering real particle arrangements made it possible to examine the role of the material heterogeneity, in particular, the particles clustering and complex interconnected topologies, as well as the statistical aspect of fracture [17,35–41]. The latter is majorly based on the "weakest link" approach, i.e., on the probability of finding a microcrack of a critical length which would develop into the macroscopic crack [42]. It is most often described by the Weibull statistics that reflects the increase in the failure probability with the sample volume [43]. This concept allowed to characterize the dispersion of the fracture parameters as functions of the variation of the size, shape, aspect ratio, and spacing between particles (e.g., [44–47]).

One factor potentially affecting the fracture statistics however remains unstudied. More exactly, the weakest link concept implies that the fracture conditions mainly depend on the distribution of the longest preexisting cracks or the largest particles sensitive to be the first to fail. Nevertheless, another inherent reason of stochastic behavior lies in the probabilistic nature of the particle fracture itself, giving rise to variability of the failure stress even for identical particles. That is, when several particles with the same size find themselves in identical stress conditions, the choice of the particle to be cracked is haphazard and the development of the macroscopic crack may be realized via multiple paths, leading to a dispersion of the fracture parameters. The present paper examines this question using a deliberately simplified numerical model considering damage accumulation in a composite material consisting of spherical brittle particles randomly embedded in a ductile matrix and having randomly varied sizes. This simplification allows to isolate the studied factor and disregard the scatter of the fracture parameters caused by such factors as the matrix grain structure, morphology and topology of the second phase, or specimen geometry. The intrinsic stochasticity is introduced by the use of random trials to accept or reject the particle cleavage controlled by a probabilistic law, while the crack coalescence is handled by a deterministic energy-based criterion. Particular attention is paid to the effect of the shape factor of the probabilistic law on the fracture conditions and their dispersion.

Experiments on a close-to-eutectic Al-Si alloy with spheroidized Si particles as the main second phase were used for a qualitative comparison of the simulated stress-strain curves and evolution of the fraction of cracked particles with experimental observations. The reason for the choice of this alloy for mechanical tests was two-fold. On the one hand, both the mechanical properties and microstructure of Al-Si alloys have been documented in the literature due to their wide applications (e.g., [6–13,17–22,41,45]). On the other hand, it is known that heat treatment can efficiently transform the interconnected coral-like Si phase characterizing the as-cast eutectic alloy into isolated particles with close-to-spherical shape [9,32,48]. The latter feature provides an opportunity to deal with a model of "structureless" material responding to the simulation conditions.

2. Materials and Methods

2.1. Experiment

In the present work, the same cast alloy AS12 was used as in [9]. Since the aim of the experiment was to evaluate deformation behavior and damage accumulation in a generic model material composed of virtually spherical hard particles in a ductile matrix, only several relevant aspects concerning the material preparation and microstructure are provided below. More details can be found in [9,48]. The alloy contained 11.4%–11.7% of silicon and less than 0.1% of Fe as the main impurity. The slightly hypoeutectic

structure of such an alloy is composed of α-Al dendrites alloy and a coral-like three-dimensional structure in the bulk of material, as revealed by deep etching of aluminum from the surface layers (see [9], Figure 1). The supplied material was preprocessed by a heat treatment aimed at removing casting defects (porosity) that may lead to an additional variability of the material toughness and other mechanical properties. For this purpose, the samples were melted by direct solidification (Bridgman method) in an argon atmosphere with a constant solidification rate of 10 cm/h^{-1} [48]. To obtain spherical silicon particles, the samples were maintained at 560 °C for 10 days and quenched in water. Compared to a shorter one-day long treatment in [9], the resulting material showed a good reproducibility of mechanical properties, in particular, a high enough maximum elongation corresponding to fracture strain $\varepsilon > 10\%$, thus indicating stabilized α-Al matrix conditions [22,49]. Optical and electron microscopy were applied to evaluate the particles spheroidization. In addition, the JEOL 2010 FEG electron microscope (JEOL USA, Inc., Peabody, MA, USA) equipped with a scanning mode (STEM) and a standard software for particle analysis allowed to estimate that the resulting Si particles had the aspect ratio about 1.5 and the diameter d varying in the range from several to 15 μm, with the averaged equivalent diameter of approximately 10 μm. Only sparse isolated needles of the intermetallic $FeSiAl_3$ phase were found.

Flat specimens with a dog-bone shape and a $16 \times 3 \times 1.5$ mm^3 gage part were used for tensile tests. Most of tests were performed at room temperature with a constant imposed strain rate, $\dot{\varepsilon}_a = 10^{-4}$ s^{-1}, in an Instron-TT-CM-L deformation machine (Instron, Norwood, MA, USA) with the load resolution of 0.1 N and an accuracy of 0.5%. Importantly, minute series of interrupted tests were realized on half of the six tested specimens, which allowed to count the number of cracked particles at multiple strain levels. For this purpose, the specimens were mirror-polished before testing. Optical microscopy (Carl Zeiss, Jena, Germany) was applied to count cracked particles on the wide side of the gage part of the deformed samples. The presence or absence of matrix-particle decohesion was also selectively verified with the aid of STEM. The results of such control tests corroborated the data of optical microscopy (cf. [9]). The interrupted tests made it possible to provide sufficient details of the damage accumulation for the comparison with the model predictions. Finally, similar to [9], three specimens were deformed at 300 °C in order to evaluate the conditions better responding to the approximations used in the computer model described below.

2.2. Computer Model

The basic ingredients of the model were as follows:

- The specimen fracture included two processes: the accumulation of cracked particles and the final coalescence of cracks. No void growth or particle-matrix decohesion was considered. As will be further seen, this assumption agrees with the experimental data obtained at room temperature. It is also corroborated by the literature data testifying that the sphericity of Si particles enhances the resistance to decohesion at the Al/Si interface [41].
- Both the particle sizes and positions within the matrix were chosen randomly in order to highlight the stochastic properties stemming from the probabilistic nature of the particle failure without interference from a possible non-uniform repartition (clustering) of the reinforcement.
- The particle failure was considered to be a random event with the probability depending on the stress on the particle. According to the experiment, no preexisting cracks were introduced. Thus, the modeling of the particle cleavage was based on the assumption of a probabilistic rule and consideration of the load transfer from the matrix to the reinforcement when the strain is increased.
- The criterion of crack connection was based on the requirement for the elastic energy stored around two cracks to be enough to create two free surfaces in the matrix and assure the energy dissipation by the plastic deformation accommodating the near-crack stresses. The model did not distinguish explicitly the effects of the stress triaxiality, global or intervoid necking, or shear banding.

The details of this scheme are presented below. To make the interpretation as simple as possible, a quasi-two-dimensional model was explored in this work. Furthermore, although the model was not supposed to reproduce behavior of a real material, the elastic and microstructure features of the tested Al-Si alloy were used for convenience. Spherical particles were randomly embedded into a squared plate with the surface area corresponding to the volume fraction of particles in Al-Si samples, $f_0 = 0.12$, and thickness equal to the diameter d_{max} of the largest generated particle. The values of the particle area were chosen randomly over an interval corresponding to d varying from approximately 2 to 15 μm, with the mean value of 10 μm. The number of particles was taken equal to 1000. This choice was aimed at selecting the modeled section big enough to represent bulk material but small in comparison with the typical size of real samples, thus corroborating the disregard of the stress/strain heterogeneity at the global scale. The resulting sample size for the above-given f_0 and d corresponded to a 1.5×1.5 mm^2 area. The coordinates of the particles along the edges of the square were generated using uniformly distributed random numbers.

The values of the elastic constants of the matrix and spheres used in the simulations correspond to the data for Al and Si provided in Ref. [8], as presented in the Table 1. The table also provides the estimates of the energy η necessary to create two free surfaces in the matrix or in a particle and, therefore, form a crack in the corresponding material. For brittle spheres, it is simply twice the surface energy of the material. In the case of the matrix, the estimate also includes the energy dissipated due to plastic relaxation of stresses near the crack.

Table 1. Elastic constants for Al and Si and the energy dissipated upon crack formation.

Parameter	Matrix	Particles
Elastic constant, μ (GPa)	33	70
Poisson ratio, υ	0.33	0.22
Dissipated energy, η (J/m^2)	14	6

The choice of the fracture statistics for different brittle materials is still an open question [38,50]. However, as the objective of the work was not to reproduce behavior of a specific material but to explore statistical features of the fracture of a model composite material, the widely used Weibull statistic [43] was applied to calculate the survival probability $p(\sigma)$ of a particle subjected to stress σ. Accordingly, the probability for a particle to remain unbroken at a given step of computation exponentially decreases with the stress:

$$p(\sigma) = exp\left\{-(\sigma/\sigma_c)^m\right\}, \quad (1)$$

where the Weibull modulus m is a material characteristic and σ_c is a critical stress inversely proportional to the square root of the particle radius. In the present study, no explicit threshold was introduced to this expression (cf. [2], p. 433). At large m values, Equation (1) describes an almost step-wise distribution function. It becomes wider as m is decreased. Therefore, the Weibull modulus, also called "shape factor", controls the variability of the failure strength of a particle. The smaller its value, the greater the dispersion of the cleavage stress. The value of m can be as small as 2 to 5 for such brittle materials as glass or chalk, varies about 10 for Si and Si-based ceramics, and may reach 100 for steels. To model the effect of the brittleness of the second phase particles on the composite fracture resistance, m was varied in the range of 6 to 100. The m values below 6 led to a very fast fracture and were impractical for the given choice of other model parameters.

As the mean of the Weibull distribution slightly depends on m in the chosen interval, a linearized version of statistics exempt of this flaw was also tested:

$$p(\sigma) = 1, \ \sigma < \sigma_c - \delta\sigma,$$

$$p(\sigma) = 0.5(1 - \frac{\sigma - \sigma_c}{\delta\sigma}), \ \sigma_c - \delta\sigma \le \sigma \le \sigma_c + \delta\sigma, \quad (2)$$

$$p(\sigma) = 0,\ \sigma > \sigma_c + \delta\sigma,$$

Here, the relative width of $\delta\sigma/\sigma_c$ of the distribution plays the role of the inverse Weibull modulus. It was varied from 0.05 to 0.5.

The stress σ is caused by the incompatibility of plastic strain between the matrix and the particle. This difference must be compensated by an elastic stress, which is at the origin of the incompatibility stresses. It was calculated using the model [51]. Accordingly, the total stress on the particle can be expressed as follows:

$$\sigma(t) = \sigma_0 + h\varepsilon(t) + 2D\gamma\mu_m f(t)\varepsilon(t), \tag{3}$$

Here, σ_0 is the elastic limit of the matrix, h the strain hardening coefficient, $f(t)$ the current volume fraction of the survived particles, $\varepsilon(t)$ the strain, the subscript m indicates the matrix, γ is the strain accommodation factor describing the load transfer from the matrix to the particle, and D the modulus correction factor accounting for the elastic inhomogeneity. The elastic limit was varied between the typical levels of 20 to 50 MPa. The strain hardening was taken either zero or 10^3 MPa. The estimates of D and γ were taken from Ref. [51] for particles of different shapes. They can be found as follows in the case of spherical symmetry:

$$\gamma = 0.05\frac{7 - 5\nu_p}{1 - \nu_p}, \tag{4}$$

$$D = \frac{\mu_p}{\mu_p - \gamma(\mu_p - \mu_m)}, \tag{5}$$

where the subscript p stands for the particles. It can be noted that the fracture of a particle results in a decrease in $f(t)$ and, therefore, a stress repartition, so that more stress is sustained by the matrix. At the same time, it also leads to an opposite trend to a local stress increase due to a decrease in the effective cross-section which transmits the load.

As far as the criterion of cracks connection is concerned, the total energy dissipated to create a crack in the matrix is given by the effective surface density η_m represented in Table 1. The available elastic energy depends on the stress intensity factor of two particles to be connected. The condition of the matrix decohesion can be written as follows [8]:

$$\frac{1 - \nu_m^2}{E_m}(K_{I1}^2 S_1^2 + K_{I2}^2 S_2^2) = \eta_m d_{\max} L, \tag{6}$$

where E_m is the Young's modulus of the matrix, $K_I = \sigma\sqrt{\pi r}$ and $S = \pi r^2$ give the stress intensity and the cross-section area for particles with respective radius values, r_1 and r_2, L the distance between them. In the case when the connecting crack meets an uncracked particle, this condition is modified by adding to the right part of the equation the respective energy necessary to cleave the particle, also presented in the table (cf. experimental observation in [40], p. 2480).

Finally, the calculation procedure was based on an explicit iterative scheme. The strain ε is the driving parameter. It is increased with a constant rate imitating a constant strain rate test. The strain is supposed to be homogeneous, i.e., necking is neglected (see above). At each step, the stress $\sigma(t)$ is calculated using Equation (3) where $f(t)$ stands for the value averaged over the specimen. The values of σ in different cross-sections are calculated considering the area variation due to the presence of cracked particles. A random number is generated for each particle and compared to the corresponding $p(\sigma)$ value (cf. Equations (1) and (2)). If the random number exceeds the survival probability, the particle cleavage is accepted. When new cracks appear, the crack percolation criterion is checked for the "nearest neighbors" in the sense of the highest stress intensity factor. In addition, this criterion is applied to verify the condition of a crack opening towards the specimen edges.

3. Results

3.1. Experimental Evaluation of Deformation and Damage Accumulation Behavior

An example of a deformation curve and a typical dependence of the fraction of cracked particles, $\varphi(\varepsilon) = 1 - f(\varepsilon)/f_0$, at room temperature are presented in Figure 1a. The shape of the deformation curve indicates that fracture takes place without necking, revealing its almost brittle nature. Indeed, micrographs of the polished side surface showed that damage accumulation consisted in the cleavage of silicon particles (Figure 1b). Even at the latest deformation stages, decohesion between the matrix and the particles was observed very rarely. The final fracture was mainly represented by brittle cleavage, with sparse ductile ligaments between cracked particles. A detailed microstructure analysis goes beyond the aim of comparison with a generic model material and will be published elsewhere.

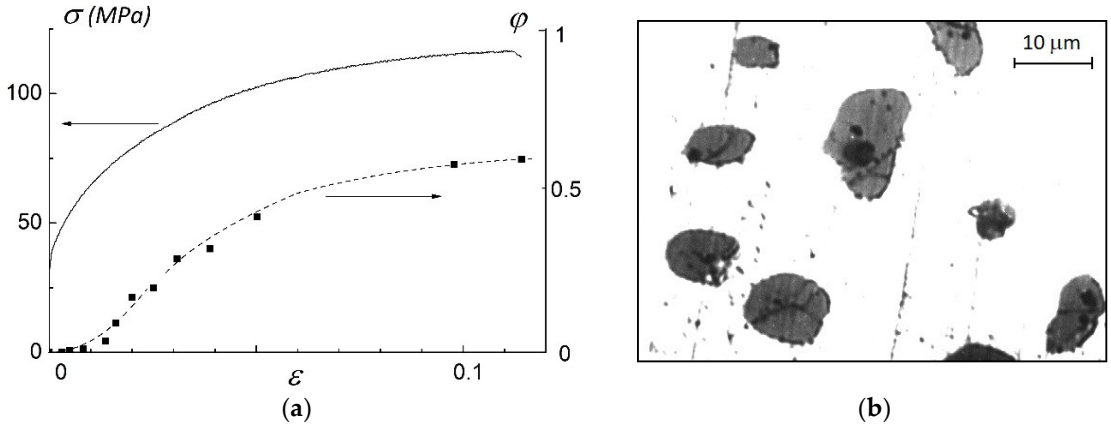

Figure 1. Deformation and damage properties at room temperature. (**a**) Example of an engineering stress-strain curve, σ(ε) and a typical strain dependence of the fraction φ of cracked particles. Squares show experimental data obtained using interrupted tests. The example of the entire deformation curve is given for another sample deformed without interruption until fracture. (**b**) Optical image of a section of the polished side surface of a deformed specimen.

At 300 °C, the material displayed more ductility and was deformed at a lower stress level (Figure 2). The highly ductile behavior is also evident from the observation of a progressive decrease in the applied stress toward zero after the onset of necking, without abrupt fracture, as contrasted with room temperature behavior illustrated in Figure 1a. It might also be noted that as in [9], "spheroidized" samples deformed at 300 °C displayed dimples on the fractured surface, as well as interface decohesion between Al and Si phases, thus corroborating the ductile nature of the fracture and indicating an important role of the local plastic deformation near Si particles because of a better matrix plasticity at high temperature (see [9–11,20,21]).

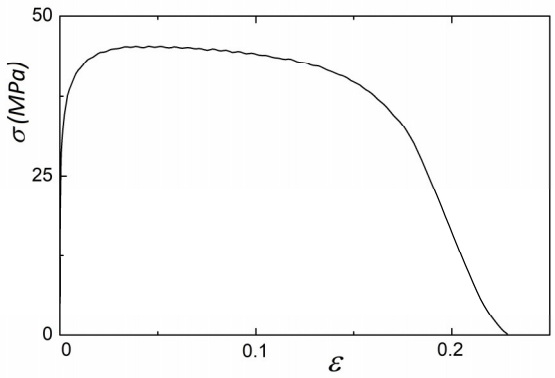

Figure 2. Example of a deformation curve at 300 °C.

It follows from this comparison that the above-proposed model would apply to room temperature, whereas decohesion between the matrix and reinforcements should be taken into account to model behavior at elevated temperatures. Accordingly, the interrupted tests aimed at following the damage evolution were performed at room temperature. For all samples, the fraction of cracked particles followed a sigmoid function, as illustrated by the example shown in Figure 1a. Although such data are rather sparse in the literature, similar dependences for spherical particles were reported in several papers, e.g., for Al-based composites reinforced with ceramic particles [37,40].

3.2. Results of Simulation

Figure 3a presents examples of simulated $\sigma(\varepsilon)$ and $\varphi(\varepsilon)$ dependences for $m = 8$, a value typical of Si [50,52]. Since plastic flow was simulated using a simplified law (Equation (3)), in particular, assuming a constant strain hardening, the model was not aimed at predicting the shape of the deformation curves and the absolute strength value. However, it correctly reproduces the feature that the stress increases until fracture despite the failure of a part of hard particles. It can be concluded that the corresponding reduction of the specimen cross-section is low enough, owing to the fact that the matrix-particle decohesion is not allowed, according to room temperature tests. Importantly, the $\varphi(\varepsilon)$-curve displays a sigmoid shape similar to the curves reconstructed experimentally. Figure 3b illustrates a spatial pattern of cracked and surviving particles and the final catastrophic crack. Overall, it can be recognized that the model captures the characteristic features of experimental observations for the Al-Si alloy, including the brittle character of fracture, the mode of damage accumulation and the behavior of strain dependences of deformation and fracture parameters (cf. Figure 1). This comparison justifies the further use of the model for a statistical study of deformation and fracture of non-homogeneous materials.

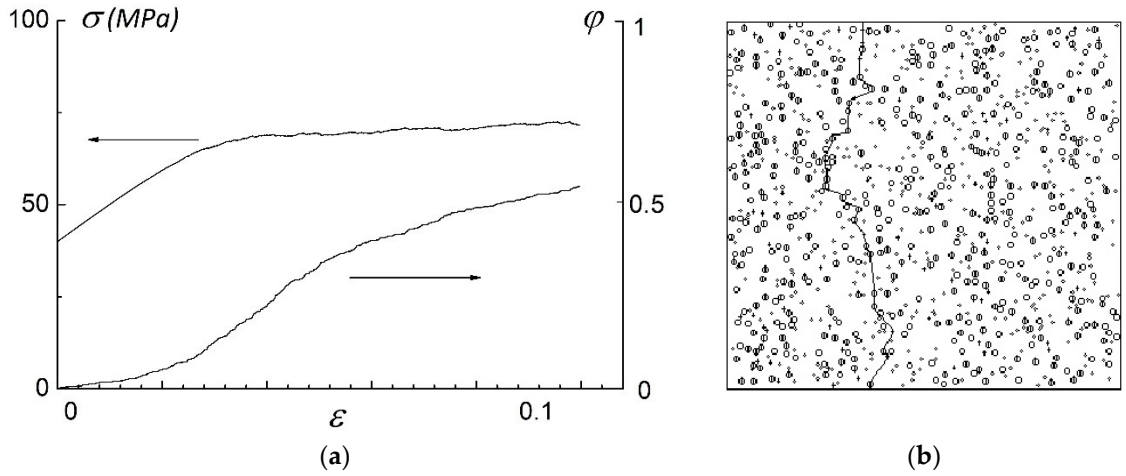

Figure 3. Example of simulation of plastic deformation and damage. (**a**) Deformation curve and strain dependence of the fraction φ of cracked particles. (**b**) Specimen face representing both cracked and surviving rigid spheres and the coalescence of cracks by matrix decohesion. $m = 8$.

Figure 4a–c illustrates the statistical distributions of the tensile strength σ_r for three values of m. The examples testify that the histograms often show a slight left-wing asymmetry somewhat varying with m. Such an asymmetry was reported in experimental investigations (e.g., [38]) and also testifies that despite the phenomenological character of the model, it correctly reproduces salient features of fracture behavior. Close-to-normal distributions were also found for some choices of the model parameters (Figure 4d). A systematic study of the shapes of histograms of various fracture parameters and their dependences on the probabilistic law goes beyond the scope of this paper. The analysis described below made use of the insignificance of the deviation from normal distributions to mimic the practical assessment of the material quality and evaluate the effects of m (or $\delta\sigma$) on the mean values

and dispersions of the σ_r, the ductility ε_r, and the fraction of cracked particles at rupture, φ_r, as well as their mutual correlations.

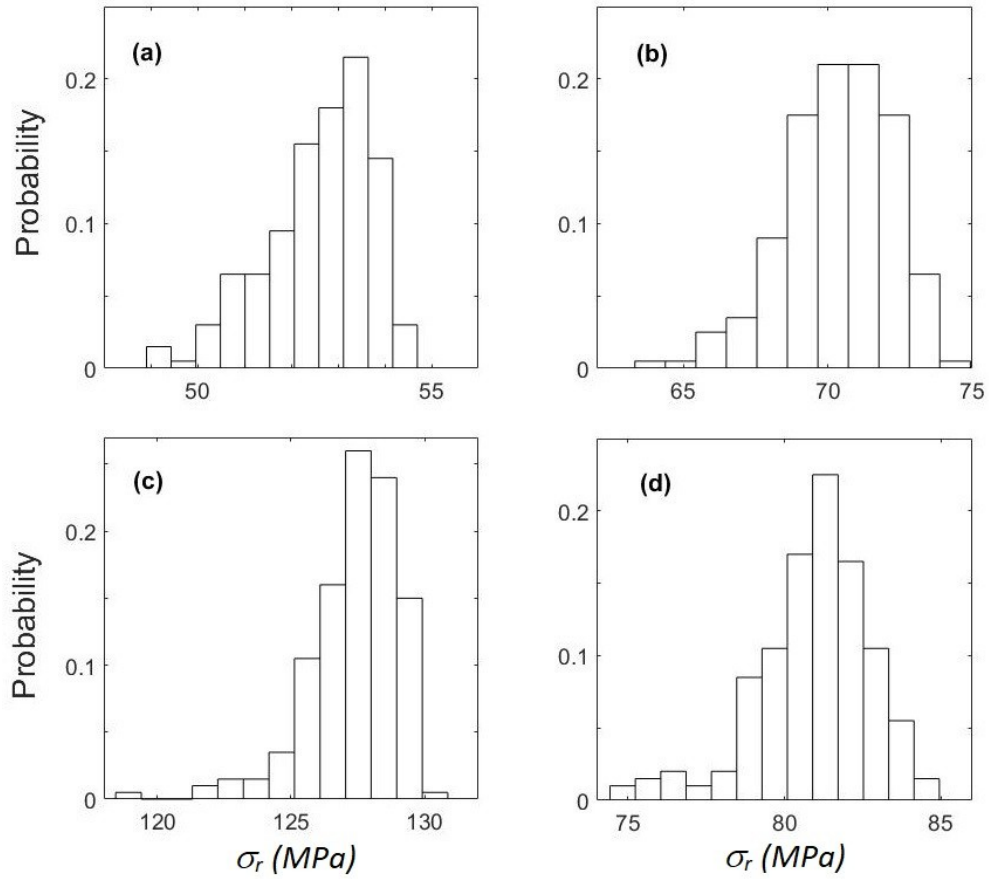

Figure 4. Examples of histograms of strength σ_r for different m-values. (**a**) $m = 6$; (**b**) $m = 10$; (**c**) $m = 50$. (**d**) Histogram obtained for arbitrarily modified values of some parameters in Equation (3) describing the coupling between the plastic flow and stress on the particles ($m = 10$).

Intuitively, it could be suggested that as far as the probability of a particle cleavage for a given $\sigma < \sigma_c$ decreases when m is increased ($\delta\sigma$ decreased), σ_r and ε_r must become higher, while φ_r and the dispersions of all parameters, $\Delta\sigma_r$, $\Delta\varepsilon_r$, and $\Delta\varphi_r$, are likely to be reduced. Indeed, if m is increased, the failure of particles starts at a higher stress level so that the criterion of Equation (6) is rapidly accomplished as soon as a few particles have been cracked. Nevertheless, the numerical simulations showed that behaviors of $\Delta\sigma_r$ and $\Delta\varepsilon_r$ do not follow this intuitive prediction in the whole range of m or $\delta\sigma$. The results of simulation illustrating the typical behavior of fracture parameters are presented in Figure 5 for both the Weibull and linearized laws.

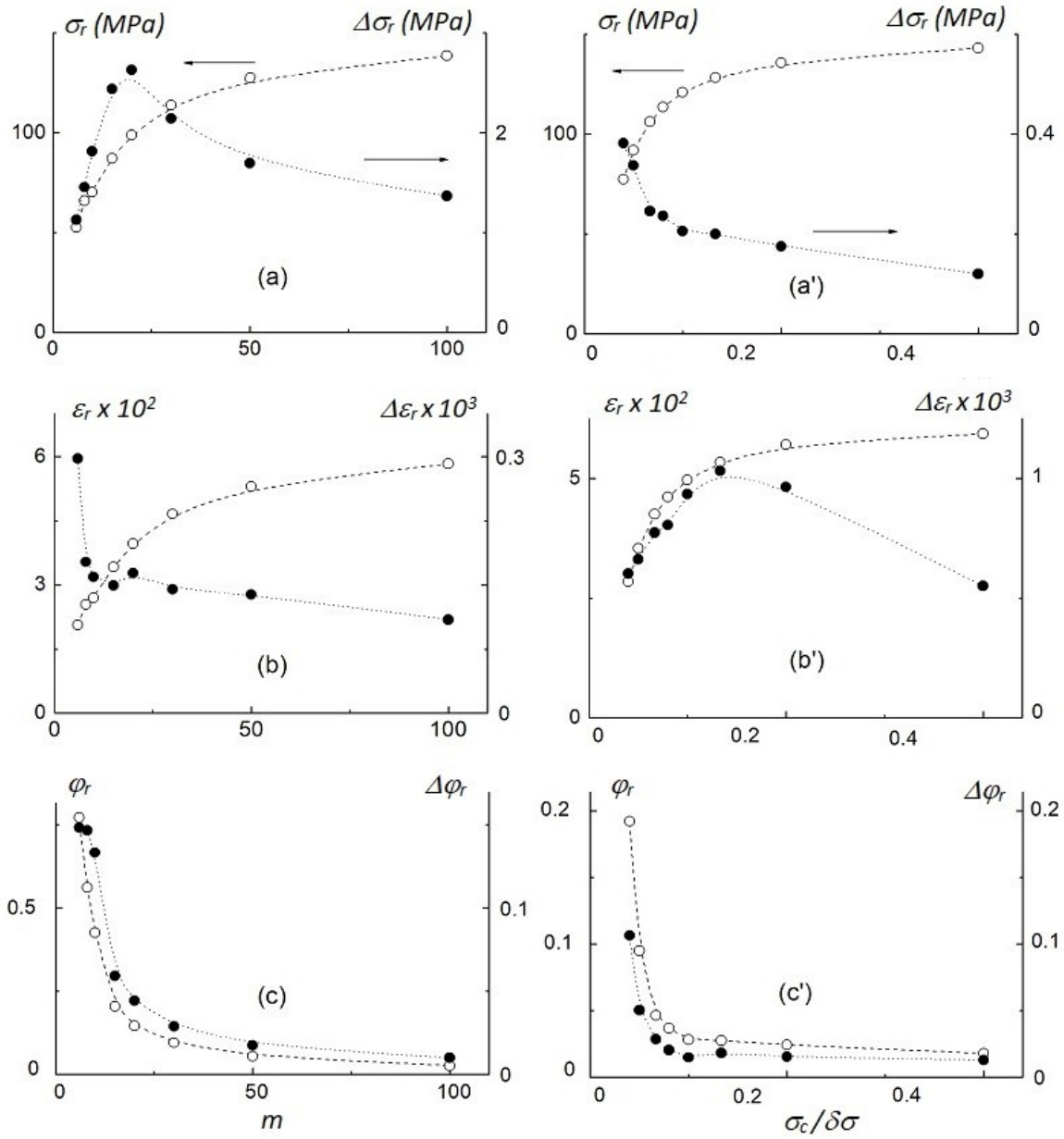

Figure 5. Simulated effects of the shape factors of the particle survival laws. Left column: results of calculation for the Weibull statistics with the shape factor m. Right column: dependences on the inverse value of the shape factor $\delta\sigma/\sigma_c$ for the linearized failure statistics. (**a**,**a′**) Mean value and dispersion of the fracture stress. (**b**,**b′**) Similar data for strain. (**c**,**c′**) Data for the fraction of cracked particles. In each chart, empty circles stand for the mean value of the studied quantity and filled circles trace its dispersion.

The data of Figure 5 testify that dispersions of the fracture stress and strain may behave non-monotonously. Moreover, the behavior may depend on the choice of the particle failure statistics. Whereas the $\Delta\sigma_r(m)$-dependence displays a maximum, $\Delta\sigma_r(\sigma_c/\delta\sigma)$ decreases monotonously. On the contrary, $\Delta\varepsilon_r$ has a maximum as a function of $\delta\sigma$ but behaves roughly monotonously with m. This result is essential for understanding that fracture emerges differently, depending on whether a large or a small part of particles is fractured before the occurrence of the conditions for a catastrophic crack.

Let us first consider the case of the Weibull statistics. It can be seen from Figure 5b that the intuitive behavior of $\Delta\sigma_r(m)$, i.e., a descending curve, corresponds to small φ values in an interval of high m. The counterintuitive dependence is associated with the fast growth of φ when m is decreased.

For example, φ is as high as 80% of the total number of particles for the smallest m (Figure 5c). These results can be explained considering the conditions at which the crack coalescence criterion is fulfilled. The dispersion of the fracture stress is due to the distributions of the particle sizes and spatial positions, which give rise to a dispersion of sizes and positions of cracks. If the number of particles is large enough, the random number generator fills the specimen with particles in a relatively uniform manner. Therefore, in the limit of high φ values, Equation (6) can be simultaneously verified in numerous sites in the specimen and there would be many possible trajectories for the crack coalescence. Thus, whenever the threshold stress for the crack coalescence is reached, the probability to find a «weak» path in the system of cracks will be similar for each calculation run. Indeed, this reasoning was corroborated by the observation of more than one catastrophic crack in the calculation runs when many particles were cleaved before reaching the coalescence condition. As a result, the smaller m, the greater φ and smaller $\Delta\sigma_r$. Were the specimen infinite, the stress dispersion would vanish in such a simple model. In the finite specimen, fluctuations in the particle distribution can lead to an appearance of a crack "percolation" path at smaller stresses, and the stress dispersion would always be finite.

In contrast to the case of Weibull statistics, the part of fractured particles only attains 20% for the least inversed value of $\delta\sigma$ in the simulations with the linear failure statistics (Figure 4c′). An explanation of this difference can stem from the fact that the particle failure probability is exactly zero below $\sigma = \sigma_c - \delta\sigma$, i.e., the linearized law contains a significant intrinsic threshold. Since there are fewer cracks, the conditions to find a percolation path are essentially modified and the behavior of the studied fracture parameters appears to be qualitatively different. For example, whereas $\Delta\sigma_r$ gradually decreases when the fracture statistics is taken sharper ($\delta\sigma$ is decreased), $\Delta\varepsilon_r$ displays a non-monotonous course. It is likely that the reason of the reduction in $\Delta\varepsilon_r$ in the limit of high $\delta\sigma$, occurring despite the decrease in the sharpness of the structure statistics, is also due to the existence of numerous crack percolation paths at high enough φ. However, such an effect is not manifested in the stress dispersion, most likely, because of the step-wise stress dependence of the failure probability.

The role of the particle cleavage statistics can also be highlighted by the analysis of correlations between various fracture parameters. In consistence with the above scenario, examples of Figure 6 bear witness to strong correlations at small m values, i.e., when the final catastrophic crack occurs in the material with multiple broken particles. When m is increased and fewer cracks are present, the failure becomes more casual. Therefore, the correlation degrades and gradually disappears. The correlation was also found to be much less pronounced in the case of the linear survival probability, even at large $\delta\sigma$.

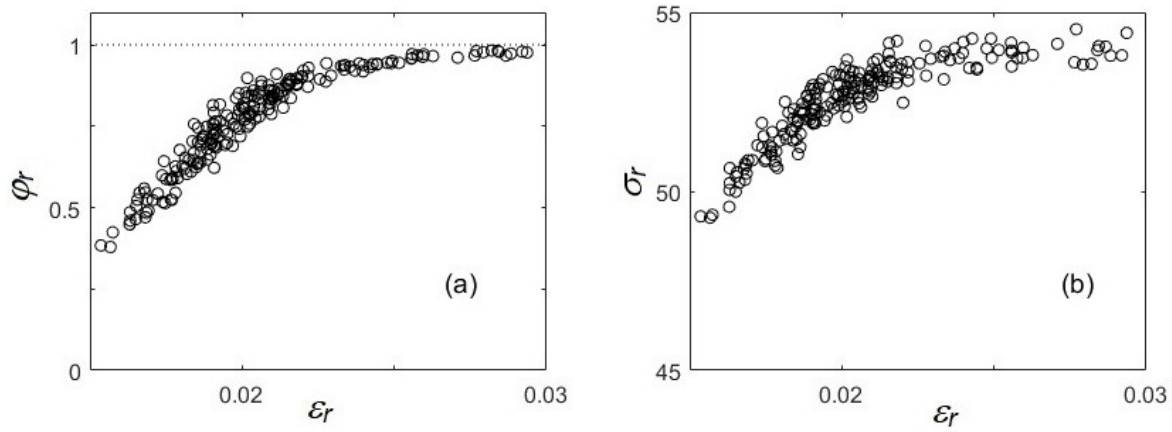

Figure 6. Correlations between the fracture parameters. (**a**) Cross-plot for the fraction of cracked particles and strain at fracture. (**b**) Similar plot for the fracture stress and strain. The statistics was obtained from 200 simulation runs for the Weibull modulus $m = 6$.

The dependences in Figure 6 allow for some quantitative corollaries. Since all particles would be fractured at infinite strain so that φ must tend to unity with increasing strain, a functional dependence can be searched for the $\varphi_r(\varepsilon_r)$-curve in the form $1-\varphi_r \propto \varepsilon_r^{-\beta}$. Averaging the data of Figure 6a in narrow intervals and replotting the average values in the double logarithmic coordinates testify that indeed, the obtained dependence is linear, i.e., obeys a scaling law in a notable interval of not very small ε_r (Figure 7a). Similar behaviors were found for other choices of $m \leq 10$ characterized by a significant data scatter that made possible such verifications. Furthermore, as the strain hardening is strongly reduced when all particles are fractured, fracture stress can also be supposed to tend to some level, σ*, at infinite ε_r. This limit can be evaluated by extrapolating the corresponding dependences to zero inverse strain. Using the as-obtained σ*, it was found that the $\sigma_r(\varepsilon_r)$-dependences also agree with the existence of a scaling function, $\sigma* - \sigma_r \propto \varepsilon_r^{-\tau}$ (Figure 7b).

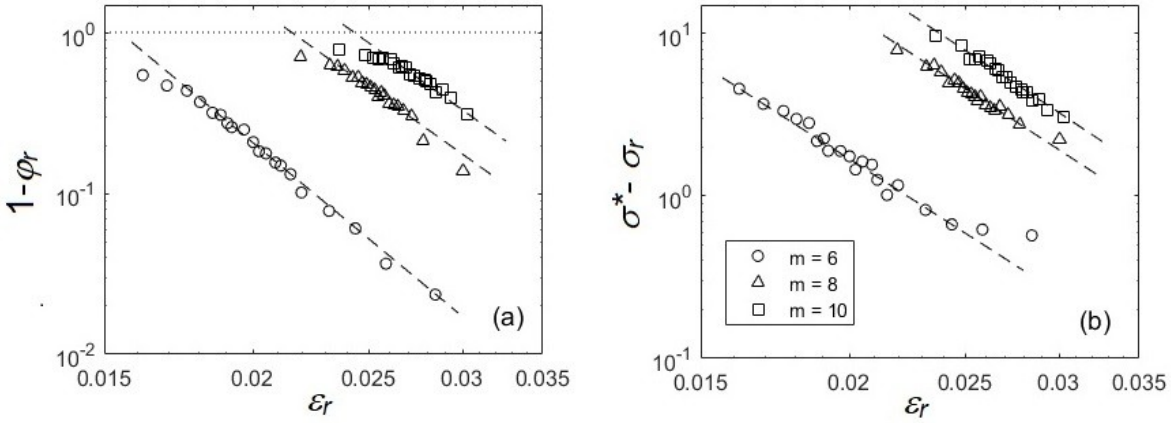

Figure 7. Scaling behavior of the fracture parameters. (**a**) Log-log dependences for the averaged $\varphi_r(\varepsilon_r)$ data of Figure 6a and similar datasets corresponding to other choices of (low) m values. The estimates of their slopes render the power-law exponent β about 6 for $m = 6$ and 5 for $m = 8$ and $m = 10$. (**b**) Similar plots for $\sigma_r(\varepsilon_r)$-data. The corresponding slope τ varies around 5.

4. Discussion and Conclusions

The paper considers a simple phenomenological model of failure of a generic "structureless" material composed of spherical brittle particles embedded in a ductile matrix (The interest of such simple microstructures is far from being purely academic. For example, recent studies of interconnected systems showed that the local loss of connectivity of the second phase allows for plastic deformation accommodating overstresses generated by the damage and, therefore, may increase the material ductility [20]), designed to highlight its intrinsic stochastic properties caused by the probabilistic nature of the particles cleavage. More specifically, the probabilistic laws, either the Weibull statistics or a linearized rule, are not applied to the entire sample, based on the weakest-link concept [2,43], but to the brittle particles themselves. This approach takes into consideration the fact that the choice of the cracks' coalescence path is not unique because the particles do not break at a well-defined local stress. The comparison of the simulation results with the deformation curves and the evolution of the fraction of broken Si particles in an Al-Si alloy deformed at room temperature testifies that the model correctly captures qualitative features of fracture of such composites in the conditions corresponding to near-brittle behavior. In particular, detailed interrupted tests allowed to closely follow in the experiment the damage accumulation as a function of plastic strain. The results clearly showed a sigmoid shape of the function describing the evolution of the number of cracked particles in the alloy used in this work. Similar behavior was earlier reported in the literature for spherical reinforcements (e.g., [37,40]), although dependences distinct from the sigmoid shape were also observed [34,45]. Importantly, such a shape naturally occurs in the studied model as a direct consequence of the probabilistic rule controlling the particles cleavage.

The model is then used to predict statistical properties of fracture using the Weibull and the linearized statistics of particle survival. One of the major simulation results is that the choice of the material of the reinforcement may strongly influence on the scatter of fracture parameters and, therefore, predictability of failure of real composite. Using the Weibull probabilistic law for particle failure, a low dispersion of the material strength was found in two opposite limits. In the case of a large volume fraction of broken particles (low Weibull modulus), the energy criterion of crack coalescence is accomplished in many sites in the specimen. The fracture stress is similar in different runs and its scatter is low. In the opposite case of a small fraction of broken particles (high Weibull modulus), the dispersion is also low because the stress grows rapidly, so that the energy criterion is satisfied in a narrow stress interval after a few cracks have appeared. The dispersion of the fracture stress can display a maximum in an intermediate range of the sharpness of the particle failure statistics. It should be noted that such a reasoning must be used with caution in the high-m limit ("soft" reinforcements) because the model does not consider plastic relaxation processes explicitly. However, the prediction using typical parameters for Al and Si suggests that a maximum may occur in practice for composites with certain combinations of the soft matrix and hard reinforcements. In particular, it may be supposed that the poor reliability of Al-Si composites, often ascribed to the foundry technology imperfectness, such as porosity, may also have a fundamental cause stemming from the fracture statistics. It should however be remarked that the simulations realized in this work do not attest the non-monotonous dependences of scatter on the shape factor of the probabilistic law as a basic feature of the composite fracture. Indeed, the maximum can be suppressed by choosing such mechanical parameters that the stress would rapidly reach high values for the given (not necessarily high) value of m, so that a crack percolation path would be found for small enough φ. Overall, the results of simulation suggest a possible need of materials selection to search for optimum matrix/reinforcement combinations.

The application of the alternative statistics of particle survival, based on a piecewise linear function, demonstrated that although the basic processes are qualitatively the same in two considered cases, the assumption of a specific probabilistic law may be crucial for the quantitative predictions of the fracture statistics because of the different rates of damage accumulation. Indeed, a monotonous dependence of strength on the shape factor of the probabilistic law was found in this case. At the same time, a maximum occurred in the similar dependence for the fracture strain.

Strong correlations between fracture parameters were found in the practically meaningful case of relatively low values of the Weibull modulus ($m \leq 10$). Moreover, the simulation results testify to the existence of scaling laws relating various fracture parameters. These relationships deserve detailed investigations in view of the prediction of fracture of particle-strengthened materials, in particular, for different particle failure statistics. It must be underlined that such a simple model cannot predict real behaviors. However, the results of the quantitative analysis attract attention to additional avenues to be explored.

In summary, although an experimental justification of the statistical predictions would be highly laborious, the observed features of the phenomenological model allow to identify methods of their verification in the framework of more realistic models of material plasticity and fracture. Notably, a systematic study of the shapes of histograms of fracture parameters is of great interest.

Author Contributions: Conceptualization, M.L.; Formal analysis, M.L. and T.L.; Investigation, M.L.; Methodology, M.L.; Software, M.L.; Validation, T.L.; Visualization, T.L.; Writing—original draft, M.L.; Writing—review & editing, M.L. and T.L.

Funding: This research was partly funded by the French State through the program "Investment in the future" operated by the National Research Agency and referenced as LabEx DAMAS [ANR-11-LABX-0008-01].

Acknowledgments: M.L. acknowledges Yves Bréchet for inspiring discussions and for providing Al-Si samples.

Conflicts of Interest: The authors declare no conflict of interest. The funders had no role in the design of the study; in the collection, analyses, or interpretation of data; in the writing of the manuscript, or in the decision to publish the results.

References

1. Ashby, M.F.; Jones, D.R.H. *Engineering Materials 2, An Introduction to Microstructure, Processing and Design*, 1st ed.; Pergamon press: Oxford, UK, 1986.
2. Pineau, A.; Benzerga, A.A.; Pardoen, T. Failure of metals I: Brittle and ductile fracture. *Acta Mater.* **2016**, *107*, 424–483. [CrossRef]
3. Pineau, A.; Benzerga, A.A.; Pardoen, T. Failure of metals III: Fracture and fatigue of nanostructured metallic materials. *Acta Mater.* **2016**, *107*, 508–544. [CrossRef]
4. Pardoen, T.; Dumont, D.; Deschamps, A.; Brechet, Y. Grain boundary versus transgranular ductile failure. *J. Mech. Phys. Solids* **2003**, *51*, 637–665. [CrossRef]
5. Zhemchuzhnikova, D.; Lebyodkin, M.; Yuzbekova, D.; Lebedkina, T.; Mogucheva, A.; Kaibyshev, R. Interrelation between the Portevin—Le Chatelier effect and necking in AlMg alloys. *Int. J. Plast.* **2018**, *110*, 95–109. [CrossRef]
6. McLellan, D.L. Modeling microstructural characteristics of Al-Si-Mg castings to develop product assurance. *AFS Trans.* **1982**, *90*, 173–191.
7. Meyers, C.W. Solution Heat Treatment Effects on Ultimate Tensile Strength and Uniform Elongation in A357 Aluminum Alloys. *AFS Trans.* **1986**, *94*, 511–518.
8. Moccelin, A.; Bréchet, Y.; Fougères, R. Fracture of an Osprey^{TM} A1SiFe alloy: A microstructure based model for fracture of microheterogeneous materials. *Acta Metall. Mater.* **1995**, *43*, 1135–1140. [CrossRef]
9. Lebyodkin, M.; Deschamps, A.; Bréchet, Y. Influence of second-phase morphology and topology on mechanical and fracture properties of Al-Si alloys. *Mater. Sci. Eng. A* **1997**, *234–236*, 481–484. [CrossRef]
10. Asghar, Z.; Requena, G.; Boller, E. Three-dimensional rigid multiphase networks providing high-temperature strength to cast AlSi10Cu5Ni1-2 piston alloys. *Acta Mater.* **2011**, *59*, 6420–6432. [CrossRef]
11. Asghar, Z.; Requena, G.; Zahid, G.H. Effect of thermally stable Cu- and Mg-rich aluminides on the high temperature strength of an AlSi12CuMgNi alloy. *Mater. Charact.* **2014**, *88*, 80–85. [CrossRef]
12. Zamani, M.; Seifeddine, S.; Jarfors, A.E.W. High Temperature tensile deformation and failure mechanisms of an Al-Si-Cu-Mg cast alloy—The microstructural scale effect. *Mater. Des.* **2015**, *86*, 361–370. [CrossRef]
13. Wang, M.; Pang, J.; Qiu, Y.; Liu, H.; Li, S.; Zhang, Z. Tensile Strength Evolution and Damage Mechanisms of Al–Si Piston Alloy at Different Temperatures. *Adv. Eng. Mater.* **2018**, *20*, 1700610. [CrossRef]
14. Butcher, C.; Chen, Z.; Worswick, M. Integration of a particle-based homogenization theory into a general damage-based constitutive model to improve the modelling of void nucleation to coalescence. *Acta Mech.* **2013**, *224*, 139–156. [CrossRef]
15. Tekoglu, C.; Hutchinson, J.W.; Pardoen, T. On localization and void coalescence as a precursor to ductile fracture. *Philos. Trans. R. Soc. A Math. Phys. Eng. Sci.* **2015**, *373*, 20140121. [CrossRef]
16. Hannard, F.; Pardoen, T.; Maire, E.; Le Bourlot, C.; Mokso, R.; Simar, A. Characterization and micromechanical modelling of microstructural heterogeneity effects on ductile fracture of 6xxx aluminium alloys. *Acta Mater.* **2016**, *103*, 558–572. [CrossRef]
17. Hannard, F.; Simar, A.; Maire, E.; Pardoen, T. Quantitative assessment of the impact of second phase particle arrangement on damage and fracture anisotropy. *Acta Mater.* **2018**, *148*, 456–466. [CrossRef]
18. Kruglova, A.; Engstler, M.; Gaiselmann, G.; Stenzel, O.; Schmidt, V.; Roland, M.; Diebels, S.; Mücklich, F. 3D connectivity of eutectic Si as key property defining strength of Al-Si alloys. *Comput. Mater. Sci.* **2016**, *120*, 90–107. [CrossRef]
19. Pathak, N.; Butcher, C.; Worswick, M.J.; Bellhouse, E.; Gao, J. Damage Evolution in Complex-Phase and Dual-Phase Steels during Edge Stretching. *Materials* **2017**, *10*, 346. [CrossRef] [PubMed]
20. Bugelnig, K.; Germann, H.; Steffens, T.; Sket, F.; Adrien, J.; Maire, E.; Boller, E.; Requena, G. Revealing the effect of local connectivity of rigid phases during deformation at high temperature of cast AlSi12Cu4Ni(2,3)Mg alloys. *Materials* **2018**, *11*, 1300. [CrossRef]
21. Bugelnig, K.; Sket, F.; Germann, H.; Steffens, T.; Koos, R.; Wilde, F.; Boller, E.; Requena, G. Influence of 3D connectivity of rigid phases on damage evolution during tensile deformation of an AlSi12Cu4Ni2 piston alloy. *Mater. Sci. Eng. A* **2018**, *709*, 193–202. [CrossRef]
22. Ceschini, L.; Morri, A.; Toschi, S.; Bjurenstedt, A.; Seifeddine, S. Influence of sludge particles on the fatigue behavior of Al-Si-Cu secondary aluminium casting alloys. *Metals* **2018**, *8*, 268. [CrossRef]

23. Rice, J.R. A Path Independent Integral and the Approximate Analysis of Strain Concentration by Notched and Cracks, J. *Appl. Mech.* **1968**, *35*, 379–386. [CrossRef]
24. Gurson, A.L. Continuum Theory of Ductile Rupture by Void Nucleation and Growth: Part I–Yield Criteria and Flow Rules for Porous Ductile Media. *J. Eng. Mater. Technol.* **1977**, *99*, 2–15. [CrossRef]
25. Needleman, A.; Tvergaard, V. An analysis of ductile rupture in notched bars. *J. Mech. Phys. Solids* **1984**, *32*, 461–490. [CrossRef]
26. Thomason, P.F. Ductile fracture by the growth and coalescence of microvoids of non-uniform size and spacing. *Acta Metall. Mater.* **1993**, *41*, 2127–2134. [CrossRef]
27. Huang, Y.; Chandra, A.; Li, N.Y. Void-nucleation vs void-growth controlled plastic flow localization in materials with nonuniform particle distributions. *Int. J. Solids Struct.* **1998**, *35*, 2475–2486. [CrossRef]
28. Pardoen, T.; Hutchinson, J.W. An extended model for void growth and coalescence. *J. Mech. Phys. Solids* **2000**, *48*, 2467–2512. [CrossRef]
29. Zhang, Z.L.; Thaulow, C.; Ødegård, J. A complete Gurson model approach for ductile fracture. *Eng. Fract. Mech.* **2000**, *67*, 155–168. [CrossRef]
30. Besson, J. Continuum Models of Ductile Fracture: A Review. *Int. J. Damage Mech.* **2010**, *19*, 3–52. [CrossRef]
31. Benzerga, A.A.; Leblond, J.B. Ductile fracture by void growth to coalescence. *Adv. Appl. Mech.* **2010**, *44*, 169–305. [CrossRef]
32. Ogris, E.; Wahlen, A.; Lüchinger, H.; Uggowitzer, P.J. On the silicon spheroidization in Al-Si alloys. *J. Light Met.* **2002**, *2*, 263–269. [CrossRef]
33. Hull, D.; Clyne, T.W. *An Introduction to Composite Materials*, 2nd ed.; Cambridge University Press: Cambridge, UK, 2003.
34. Zhao, D.; Tuler, F.R.; Lloyd, D.J. Fracture at elevated temperatures in a particle reinforced composite. *Acta Metall. Mater.* **1994**, *42*, 2525–2533. [CrossRef]
35. Martín-Meizoso, A.; Ocana-Arizcorreta, I.; Gil-Sevillano, J.; Fuentes-Pérez, M. Modelling cleavage fracture of bainitic steels. *Acta Metall. Mater.* **1994**, *42*, 2057–2068. [CrossRef]
36. Godse, R.; Gurland, J. A statistical model for low temperature cleavage fracture in mild steels. *Acta. Metall.* **1989**, *37*, 541–548. [CrossRef]
37. Whitehouse, A.F.; Clyne, T.W. Cavity formation during tensile straining of particulate and short fibre metal matrix composites. *Acta Metall. Mater.* **1993**, *41*, 1701–1711. [CrossRef]
38. Chen, J.H.; Wang, G.Z.; Wang, H.J. A statistical model for cleavage fracture of low alloy steel. *Acta Mater.* **1996**, *44*, 3979–3989. [CrossRef]
39. Worswick, M.J.; Chen, Z.T.; Pilkey, A.K.; Lloyd, D.; Court, S. Damage characterization and damage percolation modelling in aluminum alloy sheet. *Acta Mater.* **2001**, *49*, 2791–2803. [CrossRef]
40. Babout, L.; Maire, E.; Fougères, R. Damage initiation in model metallic materials: X-ray tomography and modelling. *Acta Mater.* **2004**, *52*, 2475–2487. [CrossRef]
41. Su, J.F.; Nie, X.Y.; Stoilov, V. Characterization of fracture and debonding of Si particles in AlSi alloys. *Mater. Sci. Eng. A* **2010**, *527*, 7168–7175. [CrossRef]
42. Beremin, F.M. A Local Criterion for Cleavage Fracture of a Nuclear Pressure Vessel Steel. *Metall. Mater. Trans. A* **1983**, *14*, 2277–2287. [CrossRef]
43. Weibull, W. A statistical theory of the strength of materials. *Proc. R. Swed. Inst. Eng. Res.* **1939**, *151*, 1–53.
44. Lewis, C.A.; Withers, P.J. Weibull modeling of particle cracking in metal-matrix composites. *Acta Metall. Mater.* **1995**, *43*, 3685–3699. [CrossRef]
45. Brechet, Y.; Embury, J.D.; Tao, S.; Luo, L. Damage initiation in metal matrix composites. *Acta Metall. Mater.* **1991**, *39*, 1781–1786. [CrossRef]
46. Maire, E.; Wilkinson, D.S.; Embury, J.D.; Fougères, R. Role of damage on the flow and fracture of particulate reinforced alloys and metal matrix composites. *Acta Mater.* **1997**, *45*, 5261–5274. [CrossRef]
47. Zhao, Y.H.; Weng, G.J. Transversely isotropic moduli of two partially debonded composites. *Int. J. Plast.* **1996**, *12*, 781–784. [CrossRef]
48. Madelaine-Dupuich, O.; Stolarz, J.; Triboulet, G.; Kurzudlowski, K.J. Solidification processing and microstructure analysis of synthetic Al-Si alloys. *Mater. Sci. Forum* **1996**, *217–222*, 219–224. [CrossRef]
49. Zykova, A.; Kazantseva, L.; Popova, N.; Vorozhtsov, A.; Kurzina, I. Influence of Modifying Mixtures on Si Crystal Formation in Al-7%Si Alloy. *Metals* **2018**, *8*, 98. [CrossRef]

50. Lu, C.; Danzer, R.; Fischer, F.D. Fracture statistics of brittle materials: Weibull or normal distribution. *Phys. Rev. E* **2002**, *65*, 067102. [CrossRef] [PubMed]
51. Brown, L.M.; Clarke, D.R. Work-hardening due to internal stresses in composite-materials. *Acta Metall.* **1975**, *23*, 821–830. [CrossRef]
52. Bohm, C.; Hauck, T.; Juritza, A.; Müller, W.H. Weibull Statistics of Silicon Die Fracture. In Proceedings of the 6th Electronics Packaging Technology Conference (EPTC 2004), Singapore, 8–10 December 2004; pp. 782–786. [CrossRef]

© 2019 by the authors. Licensee MDPI, Basel, Switzerland. This article is an open access article distributed under the terms and conditions of the Creative Commons Attribution (CC BY) license (http://creativecommons.org/licenses/by/4.0/).